Determining Brinell Hardness From Analysis of Indentation Load-Depth Curve Without Optical Measurement

Sung-Hoon Kim
e-mail: iljiok@plaza.snu.ac.kr

Eun-chae Jeon
e-mail: purelife@plaza.snu.ac.kr

Dongil Kwon
e-mail: dongilk@snu.ac.kr

School of Materials Science and Engineering,
Seoul National University, Seoul, 151-742,
Korea

Hardness tests are performed to determine not only hardness but also other properties such as strength, wear resistance, and deformation resistance. They are also performed to predict residual lifetime through analysis of the hardness reduction or hardness ratio. However, hardness tests require observation of the residual indentation, and for that reason are not widely used in industrial fields. This study thus examines obtaining Brinell hardness values without optical observation, using instead quantitative formulas and analyzing the relationship between the indentation depths from the indentation load-depth curve and mechanical properties such as the work-hardening exponent, yield strength, and elastic modulus on the basis of finite-element analysis. [DOI: 10.1115/1.1839213]

1 Introduction

Hardness tests are widely performed in order to evaluate other properties such as strength, wear resistance, and deformation resistance. They are widely used in industry because the residual lifetime of a material or structure can be predicted from its hardness value, hardness reduction, or hardness ratio. However, hardness tests are difficult to apply to industrial structures because they require optical measurement of the size of the residual imprint. Though some portable hardness testers have been devised, they are based only upon an empirical conversion formula.

Continuous indentation tests have been suggested as an alternative to hardness tests. In the continuous indentation test, the indentation load-depth curve is obtained by continuously measuring the applied load and the penetration depth during testing. Figure 1 shows the simplest load-depth curve: one loading curve and one unloading curve. Analysis of this curve makes it possible to determine various mechanical characteristics such as flow properties, hardness, residual stress, and fracture properties [1–8]. From the indentation load-depth curve, various indentation depths are defined that are related to such mechanical properties as yield strength, elastic modulus, and work-hardening exponent, where the work-hardening exponent is describable by a power law.

In this study, we utilized and quantified the connection between the load-depth curve and other mechanical properties. The size of residual imprint can be obtained from its geometrical relation to indentation depth. Therefore we were able to obtain the Brinell hardness merely from analysis of the load-depth curve, without optical observation of the residual imprint if the work-hardening exponent of material is known.

2 Theoretical Background

2.1 Conventional Brinell Hardness. The Brinell hardness test, proposed by J. A. Brinell in 1900, is widely used in industrial fields. The test consists of indenting the metal surface with a steel or tungsten carbide ball at a particular load [9], as shown in Fig. 2. The Brinell hardness number (HBW) is expressed as the load P divided by the surface area of the imprint, which is assumed spherical and of the diameter of the ball:

$$\mathrm{HBN} = 0.102 \times \frac{2L}{\pi D(D - \sqrt{D^2 - d^2})}, \tag{1}$$

where D is the ball diameter [mm], L is the test load [N], and d is the mean diameter of the imprint [mm].

2.2 Determination of Brinell Hardness Without Optical Observation

2.2.1 Indentation Load-Depth Curve. The indentation load-depth curve has two parts: loading and unloading. Three indentation depths are defined in the indentation load-depth curve, as shown in Fig. 1. The maximum depth, $h_{\max}$, is the total displacement of the material and indenter at the maximum load, $L_{\max}$, including elastic and plastic deformation. On unloading, the elastic deformation is fully recovered and the initial slope of the unloading curve is the indentation stiffness of the specimen and the indenter, S [10,11]. Therefore, the final depth, h_f, is the plastic deformation of the material.

2.2.2 Pile-Up Around Indenter. If there are no elastic deflection and pile-up effects, values for the final indentation depth, h_f, the indenter diameter, D, and the imprint diameter, d, can easily be obtained from the geometrical relationship among them after unloading, as shown in Fig. 3:

$$d = 2a^* = 2\sqrt{Dh_f - h_f^2} \tag{2}$$

Using the measured diameter of the residual imprint, the Brinell hardness value can be easily determined. However, the Brinell hardness value obtained by this procedure is generally larger than the real value, which means that the derived contact area is an underestimate. This underestimated contact area is due mainly to pile-up effects occurring during the indentation test (see Fig. 4), and pile-up must be taken into account in order to make the contact area more accurate. The increase in the contact area by pile-up is known to be a function of the work-hardening exponent, n, under maximum load, $L_{\max}$ [12–15]:

$$c^2 = \frac{a^2}{a_*^2} = f(n), \tag{3}$$

where $f(n)$ has been reported from finite-element analysis (FEA) by Hill, Matthews, etc., as

Manuscript received December 26, 2003; revision received September 9, 2004. Review conducted by: M. F. Horstemeyer.

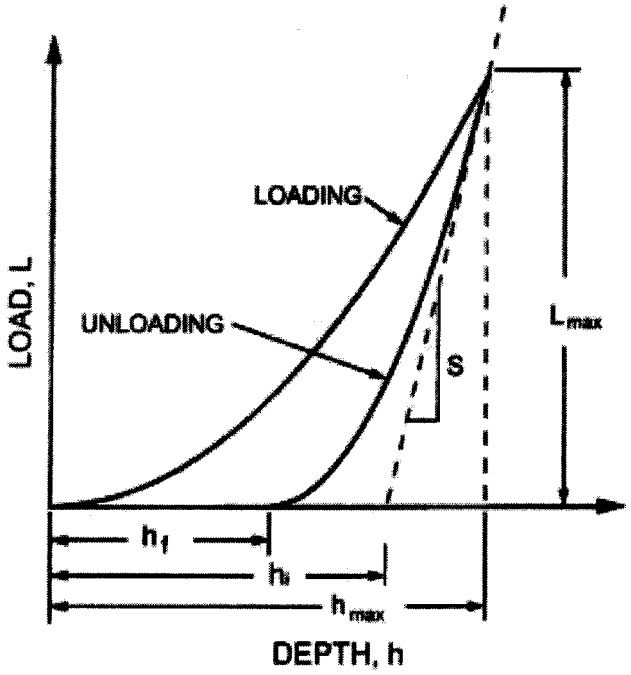

Fig. 1 The simplest load-depth curve of continuous indentation test

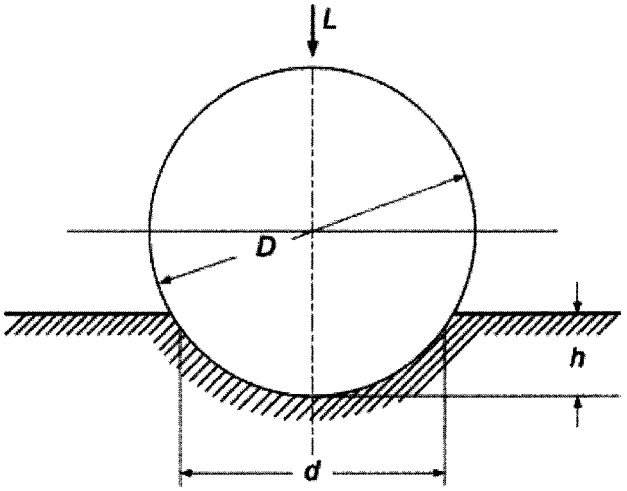

Fig. 2 Schematic diagram of Brinell hardness test

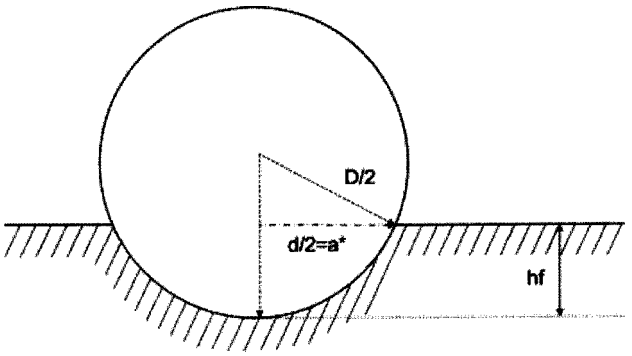

Fig. 3 Simplest indentation morphology during Brinell hardness testing

$$f(n)=\frac{5}{2}\left(\frac{2n-1}{4n+1}\right) \quad \text{Ref. [14]} \tag{4}$$

$$f(n)=\frac{1}{2}\left(\frac{2+n}{2}\right)^{2/n-2}-1 \quad \text{Ref. [15]} \tag{5}$$

In addition, it has been reported from FEA that the increase in the contact area by pile-up effects is related to the elastic modulus/yield strength ratio, E/Y, and the indentation depth/indenter diameter ratio, h_f/D, for a ball indenter [16–18]. The contact area increases with increasing E/Y and h/D due to the increase in pile-up height.

Since, however, previous research considered the pile-up effect at loaded state, the results from the research is difficult to be applied for accurately evaluating Brinell hardness that should be determined by measuring residual imprint after unloading.

3 Experimental Procedures

In this study, the 17 kinds of commonly used steels were used as testing materials (Table 1). The specimens for continuous indentation testing were cut to 25×25×20 mm, ground, and pol-

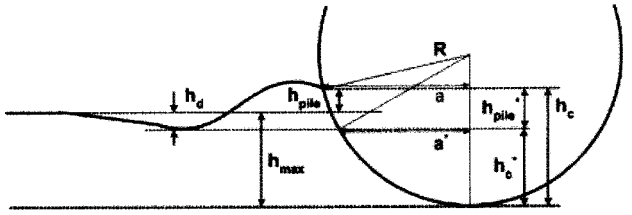

Fig. 4 Actual indentation morphology during Brinell hardness testing and definitions of various indentation depths

Table 1 Materials used in this study

API X42	API X65	KP	NAK	SA508	SCM21
Pipe steel	Pipe steel	Pipe steel	Plastic mold steel	Pressure vessel steel	Structural steel
SCM440	S45C	SK3	SK4	SKD11	SKD61
Structural steel	Structural steel	Tool steel	Tool steel	Tool steel	Tool steel
SKH51	SS400	SUJ2	SUS304	SUS316	···
Tool steel	Structural steel	Bearing steel	Stainless steel	Stainless steel	···

Table 2 Imprint diameter measured by optical microscopy and profiler

Material	API X42	API X65	KP	NAK	SA508	SCM21
d_m (mm)	0.462	0.434	0.377	0.304	0.347	0.472
Material	SCM440	S45C	SK3	SK4	SKD11	SKD61
d_m (mm)	0.363	0.444	0.464	0.451	0.388	0.431
Material	SKH51	SS400	SUJ2	SUS304	SUS316	⋯
d_m (mm)	0.408	0.532	0.435	0.448	0.470	⋯

ished with 1 μm alumina; those for tensile testing were cut into subsized cylindrical specimens of diameter 6.25 mm.

Continuous indentation tests, performed to obtain basic load-depth curves for determination of Brinell hardness, were carried out for each material using Frontics, Inc.'s AIS2000 equipment with a spherical indenter of radius 0.5 mm made of WC. Experimental conditions were selected as: maximum indentation depth 30 kgf, loading or unloading time 8 s, maximum load holding time 15 s. The maximum load was selected by a load-diameter ratio of 30 based on ASTM standard E 10.

Shape analysis is required to determine the relation between the residual imprint and indentation depths. The residual imprints were measured by a Tencor P-1 automatic long-scan profiler and an optical microscopy. The data on the residual imprints were compared with the indentation load-depth curves to derive the relation between residual imprint and indentation depth.

Such mechanical properties as yield strength, work-hardening exponent, and elastic modulus are required to describe pile-up effects around residual imprints. The yield strength and the work-hardening exponent were determined from tension testing based on ASTM standard E 8. Tension testing was performed on an Instron 5582, and the elastic modulus was determined by an ultrasonic method using a Tektronix two-channel digital real-time oscilloscope.

4 Results and Discussion

4.1 Shape Analysis of Residual Imprints

4.1.1 Measuring the Indent Size. During indentation, the indentation depth and imprint size increase with applied load, and plastic deformation, i.e. pile-up, occurs in the holding state of maximum load. During load relaxation, elastic recovery occurs, largely in direction of the load, as shown in Fig. 4.

The size of the residual imprint as measured by optical microscopy, d_m, is shown in Table 2. These values were larger than the d_{m0} values (imprint diameter on original surface) and smaller than the d_{mp} values (imprint diameter measured at the top of the pile-up).

This means that the position observed by optical measurement is neither the maximum pile-up point nor the point aligned with the original plane, but was rather a point between them. That particular point is the contact point as increased by pile-up effects, as shown in Fig. 4. Therefore, the Brinell hardness can be overestimated if h_f is used to determine the diameter.

Table 3 Radii of curvature of the residual imprints after removal of load for SKD61, SCM440, and SUJ2 steels

	h_f (μm)	d_{m0} (μm)	R (μm)
SKD61	41.77	403.70	508.60
SCM440	27.18	325.10	499.66
SUJ2	41.52	397.92	497.46

4.1.2 Geometry of the Residual Imprint. In general, plastic deformation and elastic reaction occur around the indenter under loading. Plastic deformation is seen in the pile-up phenomenon and the elastic reaction is seen in elastic deflection, as shown in Fig. 4. The elastic deflection, used to determine the precise contact area under maximum load, is recovered after unloading, during which the geometrical shape of the residual imprint may change. In particular, for Vickers hardness testing, it has been reported that the geometry of imprint is changed more by elastic depth recovery than by elastic diagonal change [19,20]. Therefore, a geometrical shape analysis of the residual imprint must be done to examine the quantitative relationship between imprint size and indentation depth for spherical indentations.

Under maximum indentation load, the geometrical shape of imprint remains spherical: a 1-mm-diameter indentation is made by a 1-mm-diameter ball. But the elastic recovery occurring after load removal may change the shape of imprint. The final indentation depth, h_f, and imprint diameter for original plane, d_{m0}, are related to radius of curvature of residual imprint, R, as follows:

$$R = \frac{h_f^2 + \left(\frac{d_{m0}}{2}\right)^2}{2h_f} \tag{6}$$

From this formula, the radii of curvature of residual imprints shown in Table 3 were determined for the three materials SKD61, SCM440, and SUJ2.

These results show that the residual imprint had a spherical shape with diameter about 1 mm. This means that the residual imprint does not change shape after load removal for a spherical indentation at 30 kgf load: elastic recovery around the indenter does not alter the shape of the residual imprint in spite of the amount of recovery at deflection depth, h_d.

4.2 Compensation for Pile-Up Effect. In general, contact area is increased by the pile-up effect. It was noted above that the quantity of the area increase is related to the work-hardening exponent, the ratio of yield strength to elastic modulus of the material, and the ratio of indentation depth, h_f, to indenter diameter, D [16,17]. The increase can be quantified by determining the pile-up height, h_{pile}, as shown in Fig. 5. The relation between h_{pile} and $h_{\max}$ under maximum load has been reported to be a function of n, E/Y, and h/D. The present study made it clear that, after unloading, h_{pile} and h_f have a similar relation to the previous relation:

$$\frac{h_{\text{pile}}}{h_f} = \frac{h_m - h_f}{h_f} = f\left(n, \frac{E}{Y}, \frac{h_f}{D}\right), \tag{7}$$

where h_m is the depth derived from the geometrical relation with diameter of residual imprint, d_m. Table 4 presents the final indentation depth, pile-up height, and mechanical properties for the 17 materials tested.

Extensive analysis of the finite-element results revealed that $(4E/Y)(h_f/D)$ correlates well with $h_{\text{pile}}/h_{\max}$ [16]. Figure 6 shows the correlation between the parameters and the mechanical properties. The pile-up parameter is linearly inversely proportional to n and $(4E/Y)(h_f/D)$. However, n and $(4E/Y)(h_f/D)$ are also linearly related. In other words, the parameters constitut-

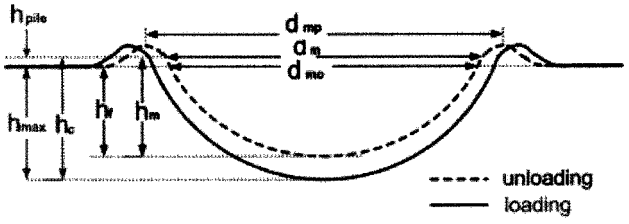

Fig. 5 Indentation morphology before and after unloading

Table 4 Analytic parameters and mechanical properties for materials in this study

	h_f (μm)	h_m (μm)	Work-hardening exponent, n	Elastic modulus E (MPa)	Yield strength, Y (MPa)
API X42	45.74	56.53	0.144	206.52	436.20
API X65	42.88	49.47	0.153	216.28	494.72
KP	30.33	36.82	0.124	211.18	764.07
NAK	18.75	23.72	0.051	202.62	1213.87
SA508	27.15	30.99	0.138	201.67	638.42
SCM21	51.09	59.19	0.206	208.83	279.53
SCM440	27.18	34.19	0.160	210.64	654.07
S45C	46.60	52.07	0.338	209.05	374.14
SK3	50.00	57.13	0.264	208.74	244.10
SK4	47.90	53.76	0.212	209.15	311.15
SKD11	35.12	39.28	0.276	215.66	242.89
SKD61	41.77	48.92	0.291	221.48	350.25
SKH51	40.31	43.51	0.259	246.80	263.85
SS400	64.65	76.61	0.234	211.26	272.70
SUJ2	41.52	49.71	0.244	214.85	322.80
SUS304	48.14	53.08	0.342	197.95	306.40
SUS316	51.15	58.67	0.281	197.16	366.65

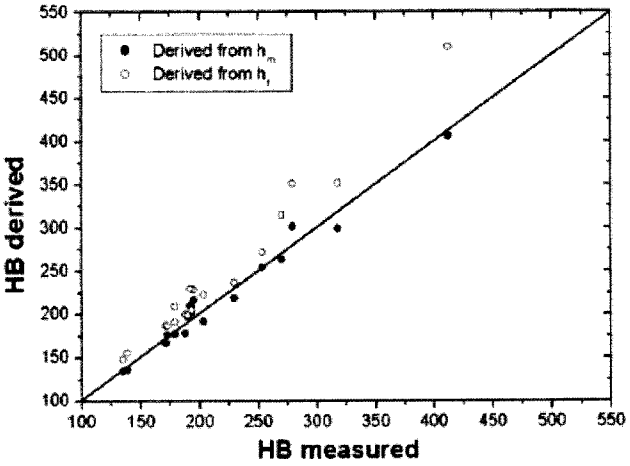

Fig. 8 Comparison of the derived Brinell hardness with the measured one

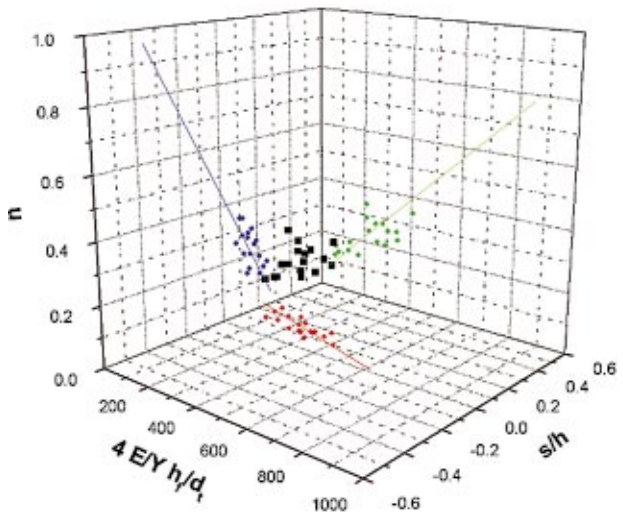

Fig. 6 Correlation between pile-up parameter, work-hardening exponent, and yield ratio-depth ratio

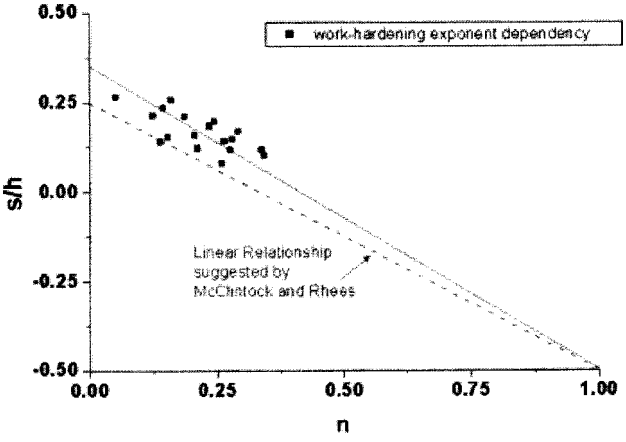

Fig. 7 Relationship between pile-up parameter and work-hardening exponent

ing the three axes of the graph are linearly proportional. Therefore, the pile-up parameter h_{pile}/h_f can be expressed as a function of the work-hardening exponent only. The pile-up parameter has a linear relationship with the work-hardening exponent for the metals studied here, as shown in Fig. 7. This result is similar to that reported by McClintock and Rhee [11] as a linear proportionality between pile-up parameter and work-hardening exponent under maximum load, described by the dotted line in Fig. 7. In particular, they suggested that the relationship was more suitable for metallic materials having a low work-hardening exponent. In addition, the results of Matthews [15] and Hill et al. [14] showed a nearly linear relation for low-work-hardening materials (below 0.3). The difference of tangents before and after unloading has an effect on elastic deflection, since the height of the pile-up, i.e., the plastic reaction of material, is unchanged after unloading but the maximum indentation depth is recovered by final indentation depth, as also reported by Taljat and Pharr [16]. The linear relationship found in this study can be quantified as

$$\frac{h_{\text{pile}}}{h_f} = -0.85768n + 0.35768 = f(n) \tag{8}$$

4.3 Determination of Brinell Hardness. On the basis of Eq. (8), the size of the residual imprint can be derived using only the work-hardening exponent and final indentation depth as follows:

$$d = 2\sqrt{Dh_f(f(n)+1) - h_f^2(f(n)+1)^2} \tag{9}$$

The Brinell hardness can be obtained from Eqs. (1) and (9), as shown in Fig. 8. If there is no pile-up around the indenter, the Brinell hardness can be derived directly from h_f (open circles in Fig. 8). These results overestimate the real Brinell hardness values as determined by optical observation. However, the Brinell hardnesses derived in this study agree well with the real data within a 5% error range (closed circles in Fig. 8). Thus we can determine Brinell hardness using only the work-hardening exponent and indentation depth, without observation of the residual imprint required in the conventional method.

Note that a material's work-hardening exponent can also be determined from continuous indentation tests using the same ball indenter as in this study [3,4,21]. The multiple-indentation load-depth curve is obtained from the test as shown in Fig. 9, and flow properties such as yield strength, tensile strength, and work-hardening exponent can easily be determined from analysis of the curve. Therefore, if the two methods are carried out side by side, the Brinell hardness test suggested in this study is more easily performed and thus more widely applicable.

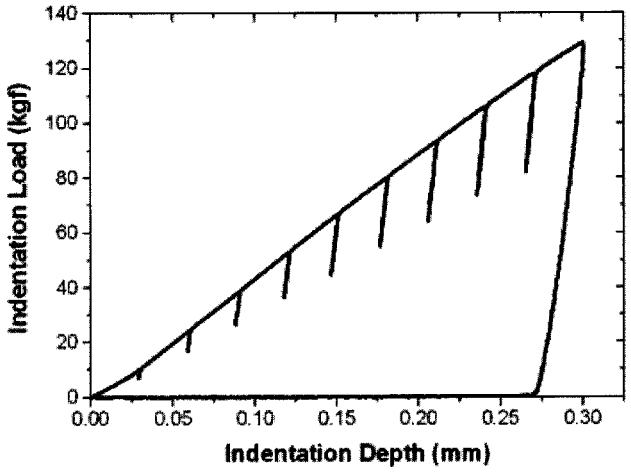

Fig. 9 General load-depth curve for evaluation of indentation tensile properties

5 Conclusions

This study introduced the continuous indentation method to overcome the shortcoming of conventional Brinell hardness testing, that it requires measurement of the residual imprint size. The Brinell hardness cannot be determined easily from the relationship between the residual imprint and final indentation depth due to the pile-up effect around the indenter. The effect of pile-up on residual imprint size was quantified from the relationship between the indentation parameters and the material's work-hardening exponent. Finally, the Brinell hardness was determined by derivation of the residual imprint size, and these results agreed well with the range actually measured. It is expected that, because of the simplicity of this method, Brinell hardness testing will be more widely used to determine the safety of industrial structures.

Acknowledgment

This research was supported by a grant (No. 04K1501-01210) from ''Center for Nanostructured Materials Technology'' under ''21st Century Frontier R&D Programs'' of the Ministry of Science and Technology, Korea.

Nomenclature

a_* = contact radius not considering pile-up
a = contact radius considering pile-up
D = indenter diameter
d = mean diameter of the imprint
d_m = mean diameter of the imprint measured by optical microscopy or profiler
d_{m0} = diameter of the imprint measured for original surface
d_{mp} = diameter of the imprint measured for the top point of pile-up
E = elastic modulus
h_d = deflection depth
h_f = final depth
$h_{\max}$ = maximum depth
h_{pile} = pile-up height
L = indentation load
$L_{\max}$ = maximum indentation load
n = work-hardening exponent
R = radius of curvature of residual imprint
Y = yield strength

References

[1] Malzbender, J., and de With, G., 2000, ''Energy Dissipation, Fracture Toughness and the Indentation Load-Displacement Curve of Coated Materials,'' Surf. Technol., **135**, pp. 60–68.
[2] Murty, K. L., Mathew, M. D., Wang, Y., Shah, V. N., and Haggag, F. M., 1998, ''Nondestructive Determination of Tensile Properties and Fracture Toughness of Cold Worked A36 Steel,'' Int. J. Pressure Vessels Piping, **75**, pp. 831–840.
[3] Ahn, J.-H., and Kwon, D., 2001, ''Derivation of Plastic Stress-Strain Relationship From Ball Indentation: Examination of Strain Definition and Pileup Effect,'' J. Mater. Res., **16**, pp. 3170–3178.
[4] Haggag, F. M., 1993, ''In-Situ Measurements of Mechanical Properties Using Novel Automated Ball Indentation System,'' ASTM STP 1204, Philadelphia, pp. 27–44.
[5] Asif, S. A. S., Wahl, K. J., and Colton, R. J., 1999, ''Nanoindentation and Contact Stiffness Measurement Using Force Modulation With a Capacitive Load-Displacement Transducer,'' Rev. Sci. Instrum., **70**, pp. 2408–2413.
[6] Lucas, B. N., Oliver, W. C., and Swindeman, J. E., 1998, ''The Dynamics of Frequency-Specific, Depth-Sensing Indentation Testing,'' *Fundamentals of Nanoindentation and Nanotribology*, N. R. Moody et al., eds., MRS, Warrendale, PA, Vol. 522, pp. 3–14.
[7] Suresh, S., and Giannakopoulos, A. E., 1998, ''A New Method for Estimating Residual Stresses by Instrumented Sharp Indentation,'' Acta Mater., **46**, pp. 5755–5767.
[8] Lee, Y.-H., and Kwon, D., 2002, ''Residual Stresses in DLC/Si and Au/Si Systems: Application of a Stress-Relaxation Model to the Nanoindentation Technique,'' J. Mater. Res., **17**, pp. 901–906.
[9] Dieter, G. E., 1988, *Mechanical Metallurgy*, McGraw-Hill, London, p. 326.
[10] Oliver, W. C., and Pharr, G. M., 1992, ''An Improved Technique for Determining Hardness and Elastic Modulus Using Load and Displacement Sensing Indentation Experiments,'' J. Mater. Res., **7**, pp. 1564–1583.
[11] Doerner, M. F., and Nix, W. D., 1986, ''A Method for Interpreting the Data From Depth-Sensing Indentation Instruments,'' J. Mater. Res., **1**, pp. 601–616.
[12] Norbury, A. L., and Samuel, T., 1928, ''The Recovery and Sinking-In or Piling-Up of Material in the Brinell Test, and the Effects of These Factors on the Correlation of the Brinell With Certain Other Hardness Tests,'' J. Iron Steel Inst., London, **117**, pp. 673–687.
[13] Rhee, S. S., and McClintock, F. A., 1962, ''On the Effect of Strain Hardening on Strain Concentrations,'' *Proc. 4th US Nat. Conf. Applied Mechanics*, ASME, Berkeley California.
[14] Hill, R., Storkers, B., and Zdunek, A. B., 1989, ''A Theoretical Study of the Brinell Hardness Test,'' Proc. R. Soc. London, Ser. A, **423**, pp. 301–330.
[15] Matthews, J. R., 1980, ''Indentation Hardness and Hot Pressing,'' Acta Metall., **28**, pp. 311–318.
[16] Taljat, B., and Pharr, G. M., 1998, ''Pile-Up Behavior of Spherical Indentations in Engineering Materials,'' Mater. Res. Soc. Symp. Proc., **522**, pp. 33–38.
[17] Alcala, J., Barone, A. C., and Anglada, M., 2000, ''The Influence of Plastic Hardening on Surface Deformation Modes Around Vickers and Spherical Indents,'' Acta Mater., **48**, pp. 3451–3464.
[18] Malzbender, J., and de With, G., 2002, ''Indentation Load-Displacement Curve, Plastic Deformation, and Energy,'' J. Mater. Res., **17**, pp. 502–511.
[19] Stiwell, N. A., and Tabor, D., 1961, ''Elastic Recovery of Conical Indentations,'' Proc. Phys. Soc. London, **2**, pp. 169–180.
[20] Cai, X., and Zhou, P. N., 1992, ''Influence of Elastic Recovery on Microindentation Hardness—A Finite Element Analysis,'' Scr. Metall. Mater., **27**, pp. 347–352.
[21] Tabor, D., 1951, *Hardness of Metals*, Clarendon Press, Oxford, p. 2.